Solution-processed infrared photovoltaic devices with >10% monochromatic internal quantum efficiency

Ahmed Maria, Paul W. Cyr, Ethan J. D. Klem, Larissa Levina, and Edward H. Sargent[a)]
Department of Electrical and Computer Engineering, University of Toronto, Toronto, Ontario M5S 3G4, Canada

(Received 21 July 2005; accepted 13 October 2005; published online 16 November 2005)

Large-area, physically flexible, solution-cast photovoltaics are of urgent interest to realize low-cost solar cells. Polymer, polymer-fullerene, and polymer-nanocrystal photovoltaics absorb light only to wavelengths as long as 750 nm, with the exception of one recent report out to 1000 nm. Half of the sun's power spectrum lies beyond 700 nm; one third beyond 1000 nm; and infrared emitters of growing interest in thermal photovoltaics emit predominantly in the 1–3 μm range. We report herein a processible infrared photovoltaic device active beyond 1 μm. Our best devices exhibit external quantum efficiencies exceeding 1% and estimated monochromatic internal quantum efficiencies greater than 10%. This represents an improvement by more than 1000 compared to the best previously reported processible >1 μm infrared photovoltaics. We employ a novel device architecture in which the infrared-absorbing active layer is based purely on semiconductor nanoparticles with no semiconducting polymer matrix. The replacement of a polymer-quantum dot composite with a pure nanoparticle layer, combined with improvements in control of organic ligands passivating nanoparticle surfaces, facilitates improved electronic transport, enhancing carrier extraction prior to recombination. © *2005 American Institute of Physics*. [DOI: 10.1063/1.2135868]

Large-area, physically flexible, solution-cast photovoltaic devices could allow solar energy to be harnessed efficiently, conveniently, and cost effectively. AM1.5 power conversion efficiencies from the best polymer,[1] polymer-nanocrystal,[2] and polymer-C_{60} (Ref. 3) photovoltaics are limited to about 3%. This arises partly from the limited efficiency with which carriers are separated and extracted before they recombine. One further barrier to achieving high power conversion efficiency is the incomplete spectral overlap between the sun's power spectrum and the absorption spectrum of typical polymers and nanocrystals used to make flexible photovoltaics. These absorb predominantly in the visible spectrum, cutting off to the blue of 750 nm. As a result, at least half of the sun's spectral power goes unabsorbed.

There are two reports in the literature of solution-cast photovoltaic devices operating in the near-infrared. A polymer/modified-fullerene photovoltaic device sensitive out to 1 μm was recently reported,[4] and there exists one report of an infrared solution-cast photovoltaic device working at wavelengths longer than 1 μm.[5] Absorption in the infrared, in this latter case, was provided by PbS (lead sulfide) colloidal nanoparticles. Through quantum size effect tuning, these nanocrystals allow the absorption onset to be selected to lie between 900 and 2000 nm, suggesting a natural means of achieving tandem or multijunction solar cells.[6] These first solution-cast photovoltaics operating beyond 1 μm exhibited short-circuit external quantum efficiencies of 0.0008%. It is of great interest to achieve efficient operation with >1 μm sensitivity. While half of the sun's AM1.5 power lies beyond 700 nm, a further third remains beyond 1 μm. Infrared heat sources that are of growing interest for thermal photovoltaic applications emit predominantly in the 1–3 μm range; these require efficient infrared photovoltaics with a corresponding spectral sensitivity.

The principal limitation on efficiency in Ref. 5 results from poor electron transport. This was indicated by a poor fill factor, a dramatic difference in quantum efficiency under modest bias versus open circuit conditions, and a rapid saturation in efficiency with increased incident power. All of these point to charge carrier extraction occurring more slowly than recombination.

In a separate series of experiments from those reported here, we have recently produced enhancements by multiple orders of magnitude in the photoconductivity of pure PbS nanocrystal films achieved through the use of new, shorter organic ligands passivating the nanoparticles' surfaces. With suitable ligands on their surfaces, PbS nanoparticles can thus provide much improved electronic transport in pure films, as required to make an efficient photovoltaic device.

Here we therefore pursue an infrared photovoltaic device in which the active layer consisted of nanocrystals alone. The photovoltaic device structure is depicted in Fig. 1. A 40 nm PEDOT:PSS layer was spin coated on top of indium tin ox-

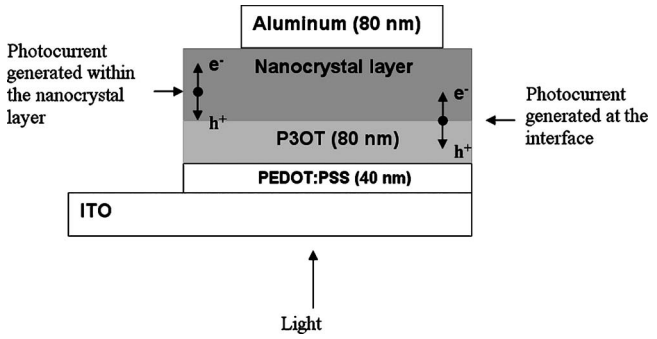

FIG. 1. Device structure. Devices A, B, and C correspond to the layer structure shown here, with the thickness of the nanocrystal layer varying from 160 down to 80 nm. In device D there was no P3OT layer.

[a)]Author to whom correspondence should be addressed; electronic mail: ted.sargent@utoronto.ca

TABLE I. Measured performance of devices A–D at 1260 nm (center of first exciton peak) illumination. The thickness of the P3OT layer was kept fixed in devices A–C. The incident optical power at 1260 nm was 166 μW.

Sample name	Sample description	Thickness of NC Layer (nm)	Fill factor	V_{oc}(V)	$I_{sc}(\mu A)$
A	P3OT/NC bilayer	160	0.32	0.26	0.51
B	P3OT/NC bilayer	115	0.3	0.12	0.46
C	P3OT/NC bilayer	80	0.4	0.02	0.16
D	Pure NC device	160	0.28	0.14	0.73

ide and baked at 120 °C for 30 min. Subsequent device processing was carried out in a N_2-filled glove box. An 80 nm P3OT layer was spin coated using a 20 mg/mL solution of P3OT in chlorobenzene. The P3OT layer was annealed for 4 min at 140 °C in a glove box. A PbS nanocrystal layer was then spin coated from a hexanes solution. Cross-sectional transmission electron microscopy images of our device showed that spin coating the nanocrystal layer from hexanes did not dissolve the bottom P3OT layer. The device was placed and kept in vacuum for 12 h before the cathode was deposited. The cathode was deposited through a mask by thermally evaporating 80 nm of Al at approximately $5e-6$ Torr followed by 150 nm of Ag at approximately the same pressure, to give devices with an area of 3 mm^2.

The nanocrystals were prepared as described in Ref. 7. As synthesized, the nanocrystals are dissolved in toluene and its surface is passivated with oleic acid ligands (18-carbon chains terminated by a carboxyl group). To facilitate electron and hole transport among nanocrystals necessary to producing a photocurrent, shorter passivating ligands are preferred. A ligand exchange was therefore carried out to replace the original oleic acid ligand with a much shorter primary butylamine ligand. The original nanocrystals were first precipitated from toluene by adding isopropanol to the solution and centrifuging. The nanocrystals were then redispersed in butylamine ligand and left at room temperature. After 2 days, the first exciton peak of the nanocrystals blue shifted by 150 nm. The exchanged nanocrystals were then precipitated by addition of isopropanol and isolated by centrifuging. The nanocrystals were then washed once with isopropanol, redispersed in hexanes, and filtered (0.2 μm) before use.

Four devices were prepared. The first three (A, B, C) were fabricated as described earlier and varied only in the thickness of their nanocrystal active layer (160, 115, 80 nm, respectively). The final device (D) had no P3OT layer; instead, its 160 nm nanocrystal active layer was deposited directly on top of PEDOT:PSS.

Table I summarizes the structure and performance of each device, reporting the measured open circuit voltage, short circuit current and fill factor at 1260 nm. For the bilayer devices A–C, the short circuit current increased monotonically as the thickness of the nanocrystal layer was increased. This indicates that at 1260 nm, the photocurrent originated primarily from the nanocrystal layer and not at the polymer-nanocrystal interface. The importance of the polymer layer to the operation of our device is seen by comparing the performance of devices A and D. Device D had a similar short circuit current and fill factor to device A, but had a smaller open circuit voltage. The main contribution of the P3OT polymer layer was, therefore, to increase the open circuit voltage of the device while keeping the fill factor and short circuit current nearly the same.

We present in Fig. 2 the external quantum efficiency (EQE) of all four devices as a function of wavelength. This measurement was carried out using a tungsten-halogen light source coupled to a monochromator whose output was focused on to the sample using a combination of lenses. The external quantum efficiency was determined based on the short circuit current and knowledge of the incident spectral power at each wavelength. Strikingly, as the wavelength of the incident light was reduced, the external quantum efficiency of device B overtook that of the thicker device A at 1100 nm, and eventually surpassed that of the pure nanocrystal device D at 920 nm. We have previously seen spectral features in photovoltaic short circuit external quantum efficiency that are not explained by changes in absorbance alone, and which must therefore relate to differences in efficiency which result when carriers are extracted following the absorption of photons of different wavelengths. In Ref. 5, the spectral variation in photocurrent coinciding with the second and third excitonic features was much more pronounced than the corresponding variation in the nanocrystal absorption spectrum, suggesting enhanced extraction of more energetic carriers.

Table II presents internal and external quantum efficiencies for devices A–D at two wavelengths. 1260 nm corresponds to the first excitonic peak, while at 720 nm, two higher-lying sets of states, the partially-spectrally overlapping second and third quantum-confined features, are absorbing with comparable contributions from each one. The inter-

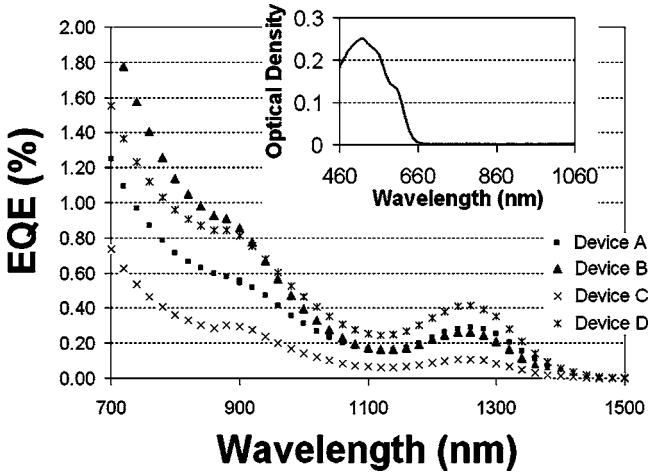

FIG. 2. External quantum efficiency as a function of wavelength for all four devices. At 1260 nm the external quantum efficiency decreases as the thickness of the nanocrystal layer is reduced. As the wavelength of the incident light is decreased, the external quantum efficiency of bilayer device B increases and overtakes that of bilayer device A (thickest) and the pure nanocrystal device D. The inset shows the absorption spectrum of P3OT. P3OT does not absorb in the wavelength region shown in the main figure.

TABLE II. Measured external (EQE) and calculated internal (IQE) quantum efficiency at the first (1260 nm) and the onset of the third exciton peaks (720 nm). The internal quantum efficiency was calculated by dividing the external quantum efficiency by the single-pass absorbance of the active layer at that wavelength.

	IQE		EQE	
Sample name	1260 nm (%)	720 nm (%)	1260 nm (%)	720 nm (%)
A	4.5	5.2	0.3	1.1
B	5.7	11.3	0.3	1.8
C	3.3	5.5	0.1	0.6
D	6.5	6.4	0.4	1.4

nal quantum efficiency of D, the pure-nanocrystal device with no P3OT layer, does not depend on the energy of the absorbing states. However, a very different situation is observed for devices A–C. This is most dramatic in the case of device B, with an intermediate (115 nm) thickness nanocrystal layer on top of P3OT. In device B, the internal quantum efficiency more than doubles at 720 nm compared to 1260 nm.

For an explanation we turn to Fig. 3. Estimates of electron affinities for P3OT and PbS nanocrystals suggest that the valence-band-to-highest occupied molecular orbital (HOMO)-level offset is at the margins between a type-I (confining) and type-II (separating) heterostructure, whereas, from the point of view of higher-lying hole states, the interface should be charge separating. We propose that holes optically excited to higher-lying states may thus be more efficiently extracted to the P3OT underlayer than those lying at the band edge. We note that this picture relies on holes remaining excited in a higher-lying state long enough that they have the chance to transfer to polymer. Intersubband relaxation times are typically thought to lie in the 100 fs–1 ps range in colloidal quantum dots and charge transfer times can be as rapid as 1 ps. It is therefore quantitatively plausible that significant charge separation occurs prior to relaxation. While differences in the transport behavior of various higher-lying excited states within quantum-confined subbands are widely used in epitaxial semiconductor devices such as long-wavelength detectors, we show here that this phenomena is also present in optoelectronic colloidal-crystal based quantum dot devices.

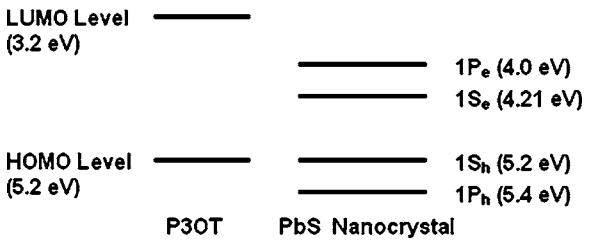

FIG. 3. Energy band diagram. On the left is the published (see Ref. 8) lowest unoccupied molecular orbital and HOMO levels for P3OT. On the right, using the same vertical vacuum reference, the first and second quantum-confined energy levels of the nanocrystals, calculated from the nanocrystals' absorption spectrum and in the approximation that the hole and electron effective masses are similar.

In sum, we achieved solution-cast infrared photovoltaic devices efficient beyond 1 μm. The best devices presented herein exhibit external quantum efficiencies exceeding 1% corresponding to estimated internal quantum efficiencies greater than 10%. We employed a novel device architecture in which the infrared-absorbing active layer was based purely on semiconductor nanoparticles with no semiconducting polymer matrix. The replacement of a polymer-quantum dot composite with a pure nanoparticle layer, combined with improvements in control of organic ligands passivating nanoparticle surfaces, facilitated improved electronic transport and thus enhanced carrier extraction prior to recombination. We also observed evidence for rapid extraction of excited (higher-lying) holes from the nanoparticles into the surrounding polymer, and attribute this observation to the alignment of the heterostructure band offsets between the polymer P3OT and the quantum-confined states inside our PbS nanoparticles.

[1]M. Granstrom, K. Petritsch, A. C. Arias, A. Lux, M. R. Andersson, and R. H. Friend, Nature (London) **395**, 257 (1998).
[2]W. U. Huynh, J. J. Dittmer, and A. P. Alivisatos, Science **295**, 2425 (2002).
[3]F. Padinger, R. S. Rittberger, and N. S. Sariciftci, Adv. Funct. Mater. **13**, 85 (2003).
[4]X. Wang, E. Perzon, J. L. Delgado, P. de la Cruz, F. Zhang, F. Langa, M. Andersson, and O. Inganas, Appl. Phys. Lett. **85**, 5081 (2004).
[5]S. A. McDonald, G. Konstantatos, S. Zhang, P. W. Cyr, E. J. D. Klem, L. Levina, and E. H. Sargent, Nat. Mater. **4**, 138 (2005).
[6]P. Peumans, A. Yakimov, and S. R. Forrest, J. Appl. Phys. **93**, 3693 (2003).
[7]M. A. Hines and G. D. Scholes, Adv. Mater. (Weinheim, Ger.) **15**, 1844 (2003).
[8]L. Micaroni, F. C. Nart, and I. A. Hummelgen, J. Solid State Electrochem. **7**, 55 (2002).